Journal of Solid State Chemistry **153,** 349–356 (2000)
doi:10.1006/jssc.2000.8781, available online at http://www.idealibrary.com on IDEAL®

Structure and Thermoelectric Properties of *Me*-Substituted $In_4Sn_3O_{12}$, *Me* = Y and Ti

W. Pitschke,*,[1] J. Werner,* G. Behr,* and K. Koumoto†

*Institut of Solid State and Materials Research Dresden, P.O. Box 270016, D-01171 Dresden, Germany; and †Department of Applied Chemistry, Graduate School of Engineering, Nagoya University, Furo-cho, Chikusa-ku, Nagoya, 464-01, Japan

Received March 29, 2000; revised May 10, 2000; accepted May 18, 2000; published online July 7, 2000

***Me*-substituted $In_4Sn_3O_{12}$, *Me* = Y and Ti, have been prepared by high-temperature solid state reaction and subsequent quenching. The structure of these compounds was analyzed using the Rietveld method. Y substitution causes an enlargement of the lattice constant whereas Ti substitution diminishes the size of the unit cell. The thermoelectric transport properties of *Me*-substituted $In_4Sn_3O_{12-\delta}$ were investigated over a temperature range of 300 to 1273 K. The electrical conductivity, σ, decreases with increasing substitution level, whereas the absolute value of the Seebeck coefficient, S, increases. Highly Ti-substituted compounds at high temperatures exhibited maximum values of the power factor $S^2\sigma$ for thermoelectric power generation of 1.9 10^{-4} W K^{-2} m^{-1} during annealing under an argon atmosphere containing less than 10 ppm oxygen. Relatively low thermal conductivities of the sintered pellets of the compounds, ca. 1.3 W m^{-1} K^{-1} at 1273 K, lead to the largest value of the thermoelectric figure of merit $Z = S^2\sigma/\kappa = 1.5\ 10^{-4}$ K^{-1} as the maximum value at 1273 K.**

Key Words: **indium tinoxide; thermoelectric properties; structure.**

INTRODUCTION

The efficiency of thermoelectric energy conversion depends on the Carnot efficiency, η_c, of the system and the thermoelectric figure of merit $Z = S^2\sigma/\kappa$ of materials constituting the thermoelectric power-generating devices, where S, σ, and κ are the Seebeck coefficient, and the electrical and thermal conductivity, respectively. Because these three parameters are closely connected with the scattering mechanism of the charge carriers and the phonons, they are dependent upon each other, and optimization of the thermoelectric performance always requires a compromise between them. Moreover, theories of conventional broad-band semiconductors predict that there is a general tendency for S and σ to vary in a reciprocal way resulting in difficult problems in the development of thermoelectric materials. The modern approaches to overcome this situation include producing materials as quantum wells or a superlattices (1), nanocrystalline composites (2), and electron-crystal, phonon-glass materials (3, 4). Since η_c of the thermoelectric system improves with increasing temperature difference, high-temperature operation is an alternative route to improve the conversion efficiency. A considerably large Z and high durability at elevated temperatures are therefore desireable for thermoelectric materials to attain highly efficient energy conversion. To date, Si–Ge alloys (5), several metal chalcogenides (6, 7), transition metal silicides (8–10), and some boron compounds (11, 12) have been developed as materials for high-temperature thermoelectric generation. Their practical utilization has been limited because many of them require complicated surface protection to prevent oxidation or vaporization, and some have essential temperature limits due to phase transitions at high temperature.

Metal oxides at their common oxidation state seem to be eminently advantageous for high-temperature operation in air, and many of these oxides have high electrical conductivities. But their mobility is orders of magnitude lower than that of common semiconductors, and therefore they have been regarded as unsuitable for thermoelectric applications. Some oxides, however, have relatively large mobilities. Recently several possible thermoelectric oxide materials have been reported, including $Nd_{2-x}Ce_xCuO_4$ (13), $La_{0.85}Sr_{0.15}CrO_3$ (14), $(ZnO)_mIn_2O_3$ (15), and $Ba_{1-x}Sr_xPbO_3$ (16). Their Z-values are smaller than those of alloys and semiconductors. Terasaki *et al.* reported that $NaCo_2O_4$ has a Z value up to $0.88 \times 10^{-4}\,K^{-1}$, almost comparable to those of conventional materials (17). However, due to the volatility of sodium and its hygroscopic nature, its practical application is limited. To find oxide materials with high thermoelectric performance for practical thermoelectric applications, further investigations are needed.

In this study, we prepared ternary and *Me*-substituted $In_4Sn_3O_{12}$, where *Me* is Y and Ti. In 1994 Ohtaki *et al.* (18)

[1] To whom correspondence should be addressed. E-mail: w.pitschke@ifw-dresden.de.

0022-4596/00 $35.00

investigated the thermoelectric properties of mixed oxides $In_2O_3 \cdot MO_x$ ($MO_x = Cr_2O_3$, Mn_2O_3, NiO, ZnO, Y_2O_3, Nb_2O_5, SnO_2). Among them are $In_2O_3 \cdot SnO_2$ consisting of In_2O_3 and a fairly large amount of $In_4Sn_3O_{12}$ providing $Z = 0.4 \times 10^{-4}\,K^{-1}$ at $T = 1273$ K. Bates *et al.* (19) determined the electrical properties of bulk $In_2O_3 \cdot SnO_2$ in air and reported an S value of $-125\,\mu V\,K^{-1}$ and an δ-value of $120\,S\,cm^{-1}$ at 1200 K for a composition of 60 mol% In_2O_3:40 mol% SnO_2 corresponding to $In_4Sn_3O_{12}$. The ternary $In_4Sn_3O_{12-\delta}$ phase is a degenerate *n*-type semiconductor with a nearly temperature independent electron concentration of $1.3 \times 10^{20}\,cm^{-3}$ and a slightly temperature dependent carrier mobility of $6.6\,cm^2/V\,s$ at 290 K, after annealing under argon. The δ value at temperatures up to 1200 K depend strongly on the oxygen partial pressure due to a small homogeneity range in the oxygen concentration of $In_4Sn_3O_{12}$ (20).

$In_4Sn_3O_{12}$ is at room temperature a metastable phase in the In_2O_3–SnO_2 system (21) with a homogeneity region ranging from 47.9 mol% to 59.3 mol% SnO_2 at temperatures above 1573 K. In thermodynamic equilibrium, the compound decomposes below 1473 K into In_2O_3 and SnO_2. By quenching, however, the compound is maintained up to room temperature. Our investigations showed the $In_4Sn_3O_{12}$ phase to remain metastable up to 1300 K during annealing under an air or Ar atmosphere.

$In_4Sn_3O_{12}$ is isostructural with a wide range of M_7O_{12} compounds that exhibit a fluorite-related superstructure (22). It crystallizes in a rhombohedral unit cell (space group *R*-3, No. 148) with $a = 0.94604$ nm and $c = 0.88584$ nm in a hexagonal basis. The unit cell contains 57 atoms arranged at four crystallographic nonequivalent positions *M*1, *M*2, O1, and O2 (M = Sn, In) (see Fig. 1). The (3*a*) *M*1 site is fully occupied by Sn cations. Their coordination is six instead of eight in the ideal fluorite structure. The configuration can be described as a distorted cube with empty anionic positions at opposite verticals. The remaining six-sevenths of *M*2 cations are in the (18*f*) general positions occupied by 33.3% Sn and 66.6% In. They are surrounded by seven oxygen atoms, set at the vertices of a highly distorted cube where one corner is lacking. The relationship to the fluorite structure is shown in Fig. 2, where the black cube is $M1O_6V_2$ (V is a vacancy in the fluorite lattice), and these vacancies are at each end of the body diagonal of the MO_8 fluorite cube (23). The white cubes are $M2O_7V$.

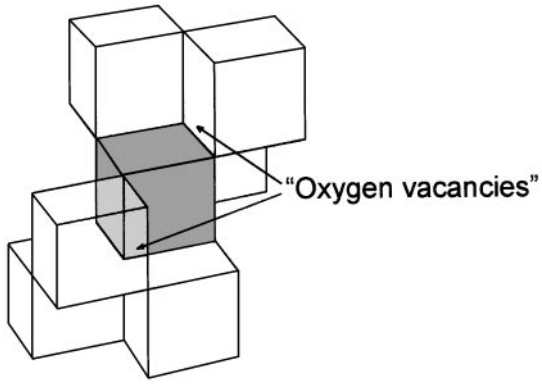

FIG. 2. Defect complex consisting of a central six-coordinated *M*1 cation surrounded by six seven-coordinated *M*2 cations (see Thornber and Bevan (23)).

The aim of this paper is to investigate the structure and the thermoelectric transport properties of ternary $In_4Sn_3O_{12}$ compounds with and without Y^{3+} and Ti^{4+} substitution.

EXPERIMENTAL

Samples of $(In_{1-x}Y_x)_4(Sn_{1-y}Ti_y)_3O_{12}$ with $x,y = 0$, 0.0125, 0.025, 0.05, 0.075, and 0.1 were synthesized by high-temperature solid state reaction of precursors made by the following procedure. For a homogeneous distribution of the dopants, the minor elements were dissolved in nitric acid first, before adding the indium and finally the tin. In this

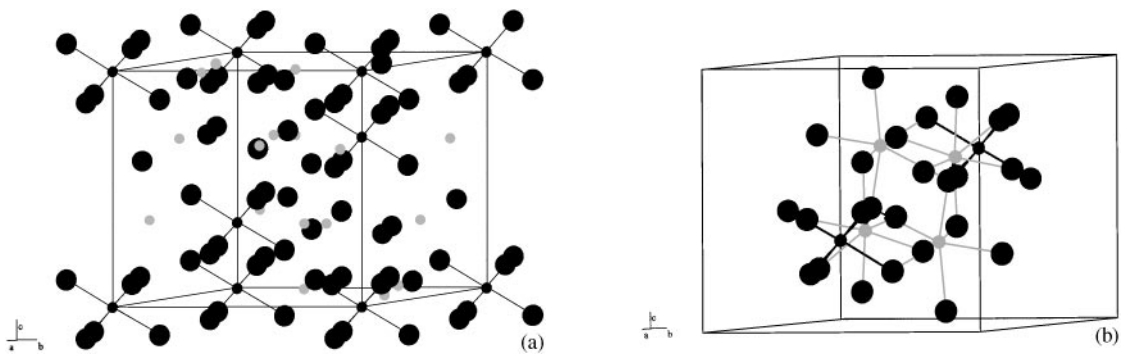

FIG. 1. (a) Hexagonal unit cell for $In_4Sn_3O_{12}$. M1–O bonds are marked as black segments. (b) M1 and *M*2 environment in $In_4Sn_3O_{12}$. Large black circles, oxygen; small black circles, *M*1; small gray circles, *M*2.

TABLE 1
Phase Composition of the Samples with the Chemical Composition $(In_{1-x}Y_x)_4(Sn_{1-y}Ti_y)_3O_{12}$

Sample	Dopant element	x/y	Phases identified by XRD
1	—	—	$In_4Sn_3O_{12}$
2	Y	0.0125	$(In_{0.9875}Y_{0.0125})_4Sn_3O_{12}$
3	Y	0.025	$(In_{0.975}Y_{0.025})_4Sn_3O_{12}$
4	Y	0.05	$(In_{0.965}Y_{0.035})_4Sn_3O_{12}$ + $In_4Sn_{3.25}Y_{0.75}O_{11}$
5	Y	0.075	$(In_{0.953}Y_{0.047})_4Sn_3O_{12}$ + $In_4Sn_{3.25}Y_{0.75}O_{11}$
6	Y	0.1	$(In_{0.944}Y_{0.056})_4Sn_3O_{12}$ + $In_4Sn_{3.25}Y_{0.75}O_{11}$
7	Ti	0.0125	$In_4(Sn_{0.9875}Ti_{0.0125})_3O_{12}$
8	Ti	0.025	$In_4(Sn_{0.975}Ti_{0.025})_3O_{12}$
9	Ti	0.05	$In_4(Sn_{0.95}Ti_{0.05})_3O_{12}$
10	Ti	0.1	$In_4(Sn_{0.9}Ti_{0.1})_3O_{12}$

case equimolar amounts of pure In (5 N), Sn (5 N), Y (3 N), and TiO_2 (4 N), respectively, were weighed, dissolved, and stirred into nitric acid, then coprecipitated with ammonia. After evaporating the liquid, the powders were fired at 500°C, then pressed into pellets at 600 MPa and reaction was sintered at 1460 ± 10°C for 32 hours. The air-fired samples were quenched in liquid nitrogen. In Table 1 the chemical compositions of the samples are given together with the phase compositions analyzed by X-ray diffraction (XRD) measurements.

The XRD data at room temperature were collected on a Philips diffractometer PW1820 using Co$K\alpha$ radiation. In order to examine the crystal structure by the Rietveld method the diffraction patterns were recorded in the range of $15^\circ < (2\Theta) < 130^\circ$ with a step size of $0.03^\circ(2\Theta)$ and a measurement time of 10 s per step. Polycrystalline Si was used for instrument calibration. The data were analyzed using the DBWS-9411 Rietveld program (24). Additionally, the chemical composition and the microstructure of chosen samples were determined by electron probe microanalysis (EPMA). The electrical measurements were carried out on specimens cut from sintered pellets as parallelepiped bars of ca $4 \times 3 \times 12$ mm^3 in size. σ and S were measured simultaneously at steady-state temperature in air and in an Ar atmosphere. σ was measured using the four-probe direct current (dc) method. Platinum plates were stuck to each end as electrodes, and two Pt leads wound around the specimen were used to measure the voltage drop. For thermopower measurements a temperature gradient was generated in the specimen by passing cool air through a quartz protection tube placed near one end of the specimen. Thermoelectromotive force measured as a function of temperature difference gave a straight line and its slope was taken as the S value.

Thermal diffusivity and specific heat were measured under vacuum by the laser flash method on disk samples 10 mm in diameter and 2 mm in thickness. The measurements were performed from room temperature up to 1200 K. A ruby laser with a pulse width of 800 μs was used as a heat source. The finite pulse width effect could therefore be neglected. An SbIn infrared detector was used at 77 K for thermal diffusivity measurements. Specific heat measurements were performed using a Pt/Pt 13% Rh thermocouple fixed on the surface of the sample. Sapphire was used as a standard for specific heat. The density of the samples was determined by the Archimedes method in water. Thermal conductivity was calculated as a product of bulk density at room temperature, thermal diffusivity, and specific heat measured on a sample.

RESULTS AND DISCUSSION

Crystal Structure

The structural data for $In_4Sn_3O_{12}$ determined by the refinement of neutron powder diffraction data (22) were used as starting values in the Rietveld refinement procedure. At first the lattice constants were refined. After that, the atomic position of the substituted ions within the unit cell was proved placing them at the (3*a*) and (18*f*) positions of the cations and refining the atomic coordinates and the occupation numbers. In both investigated types of *Me*-substituted $In_4Sn_3O_{12}$ the *Me* ions were found to be located at the (18*f*) position instead of In (Sn) in case of Y-substitution (Ti-substitution). For the Y-substituted compounds with substitution levels $x \geq 0.05$ additional reflections of a face-centered cubic phase with a lattice constant of 0.5110 nm were observed. By means of EPMA the chemical composition of this phase was determined to be approximately $In_4Sn_{3.25}Y_{0.75}O_{11}$. Rietveld refinement provides an NaCl structure for this phase with partly occupied positions analogous to Y_3C.[27]

Figures 3 and 4 show the lattice constants of *Me*-substituted $In_4Sn_3O_{12}$ and the volume of the unit cell. Substitution of In^{3+} by Y^{3+} causes an enlargement whereas substitution of Sn^{4+} by Ti^{4+} diminishes the size of the unit cell. This is caused by the larger ionic radii of Y^{3+} (1019 pm) compared to In^{3+} (920 pm), and of Ti^{4+} (740 pm) compared to Sn^{4+} (810 pm) (28). In the case of Ti-substituted compounds the lattice constants and the volume of the unit cell depend linearly on the substitution level y: $a = (0.9467 - 0.0259y)$ nm, $c = (0.8857 - 0.0060y)$ nm, and $V = (0.6875 - 0.0422y)$ nm^3. The shrinkage in the a direction is greater than that in the c direction, as opposed to Y-substituted compounds which show a greater enhancement in the c direction than in the a direction: $a = (0.9467 + 0.0204x)$ nm, $c = (0.8856 + 0.0336x)$ nm, $V = (0.6874 + 0.0558x)$ nm^3. These dependencies were determined by least-squares fitting of the first three data points

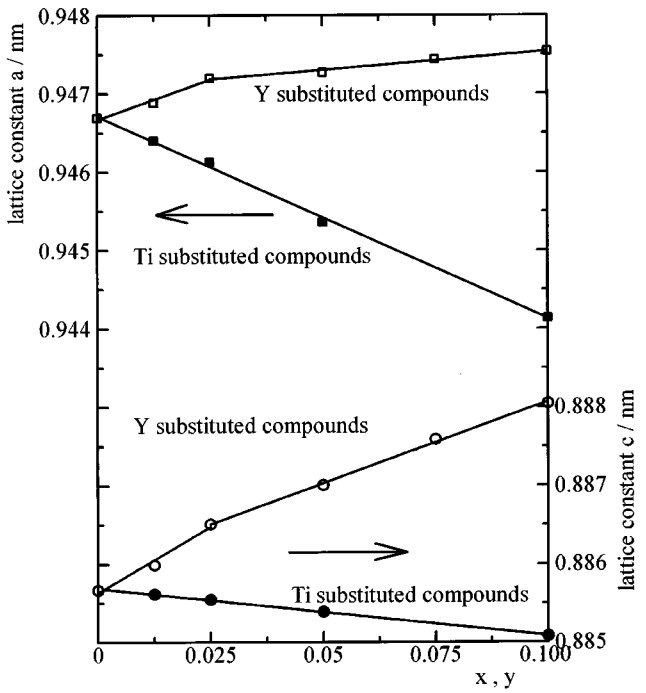

FIG. 3. Lattice constants of the $(In_{1-x}Y_x)_4(Sn_{1-y}Ti_y)_3O_{12}$ unit cell.

in the range $0 \leq x \leq 0.025$. As a result of the additional formation of $In_4Sn_{3.25}Y_{0.75}O_{11}$ at higher substitution levels Y was only partly built in the $In_4Sn_3O_{12}$ cell. Consequently the gradient of the $a(x)$, $c(x)$, and $V(x)$ curves decreases.

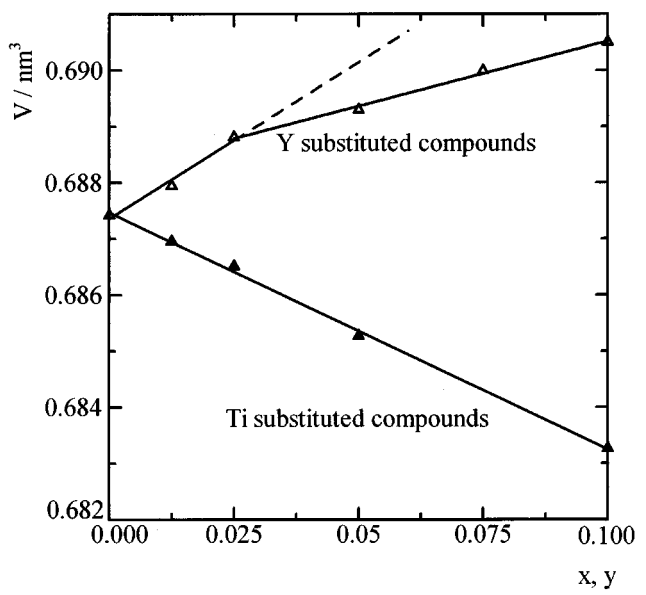

FIG. 4. Volume of the $(In_{1-x}Y_x)_4(Sn_{1-y}Ti_y)_3O_{12}$ unit cell. The dashes give the extrapolation of the line fitted to data of slightly Y-substituted compounds.

Using the extrapolation of the $V(x)$ curve to higher x one can estimate the chemical composition of the Y-substituted $In_4Sn_3O_{12}$ phase, see Table 1.

Lattice constants and atomic positions determined for $In_4Sn_3O_{12}$ agree with the results of Nadaud *et al.* (22). *Me* substitution does not influence the atomic positions within the unit cell. As a result of the changed lattice constants, however, the absolute distances between the ions vary, altering the electronic structure of the compounds.

Transport Properties

In Figure 5 σ and S for $(In_{0.975}Y_{0.025})_4Sn_3O_{12-\delta}$ obtained during the first three heating cycles in air are given. Under thermodynamic equilibrium conditions the oxygen deficit, δ depends on $(1/T)$ and $\lg(p_{O_2})$, where p_{O_2} is the oxygen partial pressure. δ increases with increasing temperature and decreasing oxygen partial pressure. In the as-prepared state the compounds show a small oxygen deficit characteristic of oxygen partial pressure of 0.2 atm and the sintering temperature of 1460°C, frozen by quenching the samples in liquid nitrogen. During the first heating cycle in air at temperatures less than 650°C, δ decreases meaning that the oxygen concentration increases. Consequently, the oxygen vacancy density (i.e., the carrier density n), and therefore σ, decrease. The process starts in a surface layer of the grains and finishes when the oxygen sublattice reaches

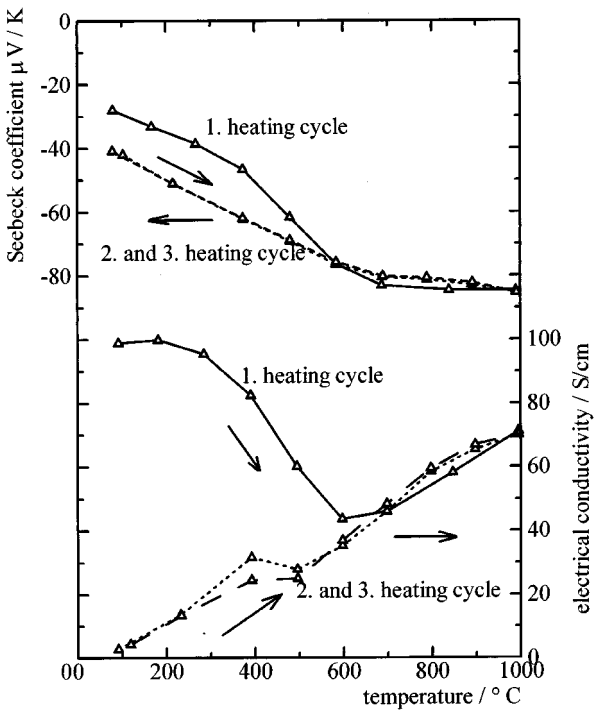

FIG. 5. Electrical conductivity and the Seebeck coefficient for $(In_{0.975}Y_{0.025})_4Sn_3O_{12}$ during the first heating cycles in air.

equilibrium. At $T > 650°C$ δ increases with increasing temperature, i.e., new oxygen vacancies are created and the carrier density n and σ increase. At the second and third heating cycle the $\sigma(T)$ and $S(T)$ curves became reproducible, indicating stationary conditions. In the low-temperature range the ionic defect equilibrium is frozen and the temperature dependence of σ, which is discussed in detail below, is determined by charge carrier depletion due to oxygen chemisorption, and scattering of the electrons by phonons and by ionized impurities. σ is less than that in the initial stage which is a direct result of the smaller carrier density and the negative value of S increases only slightly. Therefore, at temperatures below 650°C $S^2\sigma$ in the second heating cycle is less than the power factor for as-prepared samples with a lower oxygen level. This is characteristic of samples annealed at an oxygen partial pressure of 0.2 atm. A similar behaviour was observed for all the investigated compounds.

In the following the data observed after the second heating cycle under air are discussed. σ of $(In_{1-x}Y_x)_4(Sn_{1-y}Ti_y)_3O_{12-\delta}$ is given in Fig. 6. The ternary $In_4Sn_3O_{12}$ compound shows values of σ of about 50 S cm^{-1} at room temperature and about 120 S cm^{-1} at 1250 K. This is consistent with the values reported by Bates *et al.* (19). The temperature dependence of σ in the ternary compound

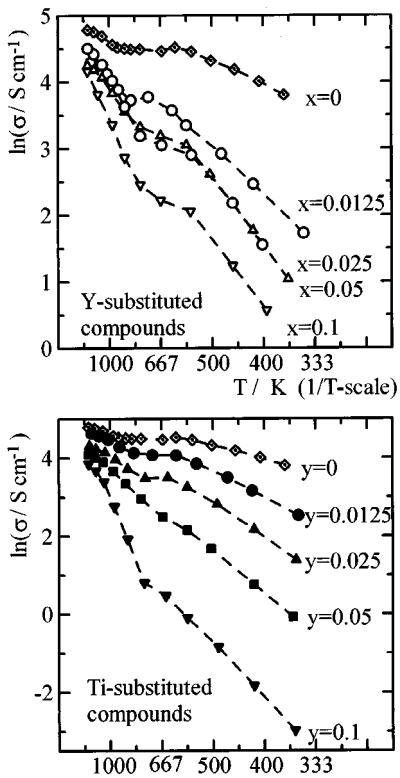

FIG. 6. Electrical conductivity for Y-substituted (open symbols) and Ti-substituted (closed symbols) $In_4Sn_3O_{12}$ annealed in air.

appears to have two transition points at about 550 and 920 K. At $T > 920$ K the oxygen in the oxygen sublattice is in balance with the atmosphere, i.e., a defect equilibrium is formed dependent on the temperature and the oxygen partial pressure. In this range the temperature dependence of $n(T)$ meets a real activation of ionic defects, whereas at lower temperatures $n(T)$ cannot respond to the oxygen partial pressure because of low kinetics. On the other hand, the temperature dependence of the carrier mobility, $\mu(T)$, is assumed to be determined by phonon scattering, i.e., in the case of a degenerated semiconductor $\mu \sim T^{-5/2}$. The relationship between $\ln(\sigma)$ and $1/T$ is therefore not linear. Between 920 K and room temperature σ is influenced by the chemisorption of oxygen and the electron system resulting from the frozen defect equilibrium. Oxygen is adsorbed at the surface of the porous sinter body and n decreases. This is a result of the electron transfer into the adsorbant, where the oxygen is chemisorbed as miscellaneous, negatively charged species (29). μ at low temperatures should be determined by phonon scattering as well as by ionized impurities for which $\mu \sim T^{3/2}$. Consequently the decreasing conductivity is mainly caused by the decreasing number of charge carriers. The lower gradient in the intermediate temperature range between 920 and 550 K is caused by two effects: the charge alteration of chemisorbed oxygen ($O^{2-} \rightarrow O^-$) and the increasing chemisorption similar to that of SnO_2 (30). In the low-temperature range the oxygen chemisorption predominates causing a stronger ascent of the $\ln(\sigma) \propto (1/T)$ curve. The σ values of the substituted samples are much lower than that of the ternary sample, which can be understood as a decrease of μ due to increasing electron impurity scattering resulting in a strong decrease of σ, especially in the low-temperature range. With increasing substitution level the lower transition point moves toward higher temperatures. In other words, with increasing substitution level, defect activation processes start at lower temperatures.

In Fig. 7 S is shown as a function of the temperature. In the range between 350 and 923 K the absolute value of the ternary compound increases monotonically from 30 μV K^{-1} up to 65 μV K^{-1}. In the high-temperature range the slope is much lower and S reaches 70 μV K^{-1} at 1200 K. The increasing negative values of S at $T < 923$ K are typical for broad-band, degenerated semiconductors. For such materials the coefficient is proportional to kT/E_f, where E_f is the Fermi energy. Above 923 K absolute values increase with less change due to the onset of the ionic defect activation process. For the Ti-substituted samples in the low-temperature range, the absolute value of S increases with increasing substitution level. The curves for highly Ti-substituted compounds show a different temperature dependence below and above about 900 K, as compared to the ternary compound. However, for the weakly substituted samples the slope in the high-temperature range is rather

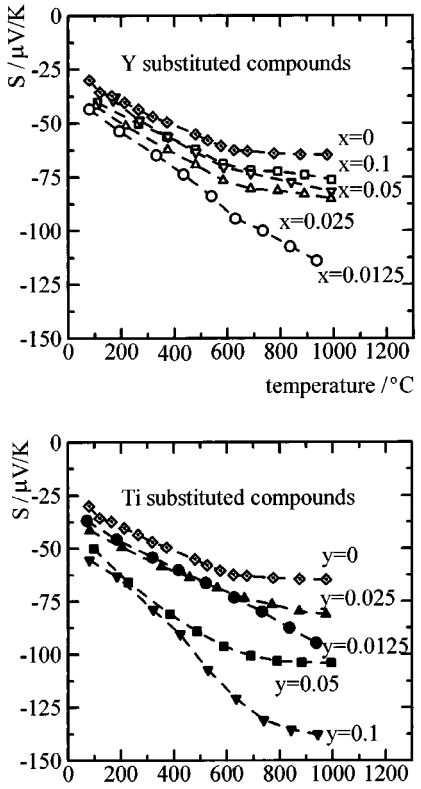

FIG. 7. Seebeck coefficient for Y-substituted (open symbols) and Ti-substituted (closed symbols) $In_4Sn_3O_{12}$ annealed in air.

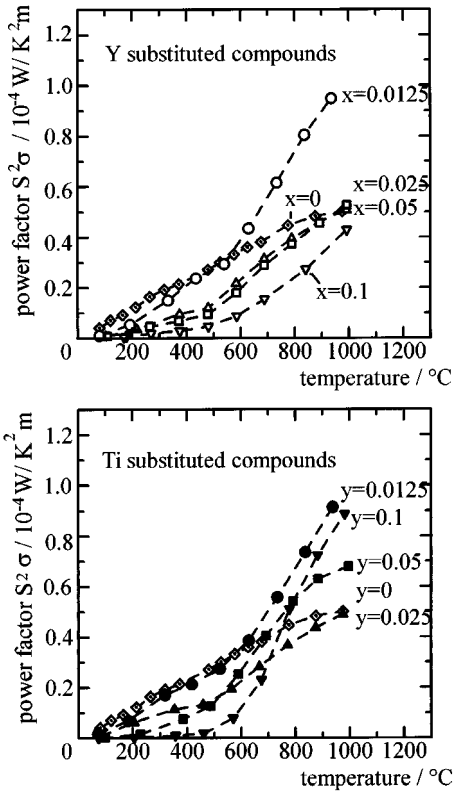

FIG. 8. Thermoelectric power factor $S^2\sigma$ for Y-substituted (open symbols) and Ti-substituted (closed symbols) $In_4Sn_3O_{12}$ annealed in air.

large. Consequently, the $In_4(Sn_{0.9875}Ti_{0.0125})_3O_{12}$ compound has S of about 90 $\mu V\,K^{-1}$ at 1200 K. This value is larger than those of the other compounds, with the exception of $(In_{0.9}Y_{0.1})_4Sn_3O_{12}$. This compound has the maximum value of S (135 $\mu V\,K^{-1}$). In the case of Y-substituted compounds, for $(In_{0.9875}Y_{0.0125})_4Sn_3O_{12}$ a similar temperature dependence was observed as for the weakly Ti-substituted compound, but with larger absolute values. As a result of the additional formation of $In_4Sn_{3.25}Y_{0.75}O_{11}$ with increasing substitution level, the value of S decreases. This effect has been previously observed for $(In_{0.985}Y_{0.025})_4Sn_3O_{12}$, which was found by XRD to contain $(In_{0.9875}Y_{0.0125})_4Sn_3O_{12}$ as a single phase. On the other hand, the detection limit of XRD is rather large, about 5 wt%, and the electric transport properties are very sensitive to small structural deviations. It is possible that a small amount of $In_4Sn_{3.25}Y_{0.75}O_{11}$ was formed in this compound, giving rise to a decrease in electrical resistivity.

Figure 8 shows, calculated from σ and S data, $S^2\sigma$. Y- and Ti-substituted compounds show smaller $S^2\sigma$ at lower temperatures. As a result of the rather large S of the weakly substituted compounds and for $(In_{0.9}Ti_{0.1})_4Sn_3O_{12}$, $S^2\sigma$ at $T > 600°C$ exceeds the values of the undoped compound.

As observed during the first heating cycle under air the thermoelectric transport properties become worse with increasing oxygen partial pressure. In order to investigate the properties of samples with low oxygen level, σ and S were measured for the ternary and the highly Ti-substituted compound annealing them under Ar atmosphere containing less than 10 ppm oxygen. The resulting curves are given in Figs. 9 and 10 together with the curves measured under air. As a result of the higher density of oxygen vacancies, (i.e., of the higher carrier density) the values of σ and S for the samples

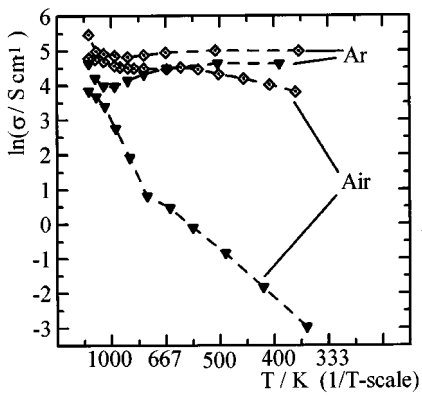

FIG. 9. Electrical resistivity for $In_4Sn_3O_{12}$ and $In_4(Sn_{0.9}Ti_{0.1})_3O_{12}$ annealed in argon and air.

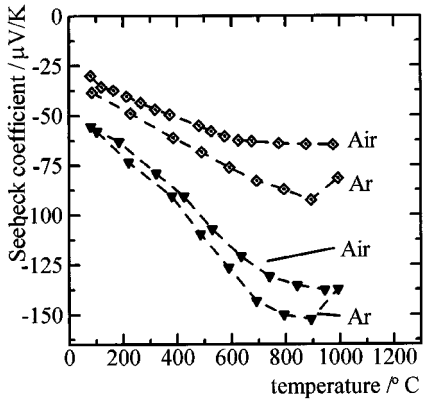

FIG. 10. Seebeck coefficient for $In_4Sn_3O_{12}$ and $In_4(Sn_{0.9}Ti_{0.1})_3O_{12}$ annealed in argon and air.

annealed under Ar are larger in the entire temperature range. The oxygen chemisorption can therefore be neglected and so at $T < 923$ K n is nearly temperature independent (20). The decrease in the electrical conductivity with increasing temperature is obviously caused by a decreasing mobility due to increasing phonon scattering of the electrons. At $T > 923$ K the activation process of ionized defects starts and again δ rises. $S^2\sigma$ of these compounds annealed under Ar atmosphere is much larger than for oxygen-rich compounds annealed under air (see Fig. 11). It monotonically increases with increasing temperature. The highly Ti-substituted compound shows maximum values of $1.9 \times 10^{-4}\,W\,K^2\,m^{-1}$.

Thermal Transport Properties and Thermoelectric Figure of Merit

In Figure 12 κ is given for the ternary and the highly substituted compounds. A rather low relative density of the sample, namely 60%, is presumably responsible for these

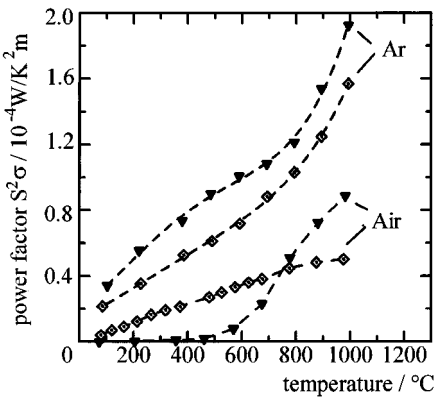

FIG. 11. Thermoelectric power factor $S^2\sigma$ for $In_4Sn_3O_{12}$ and $In_4(Sn_{0.9}Ti_{0.1})_3O_{12}$ annealed in argon and air.

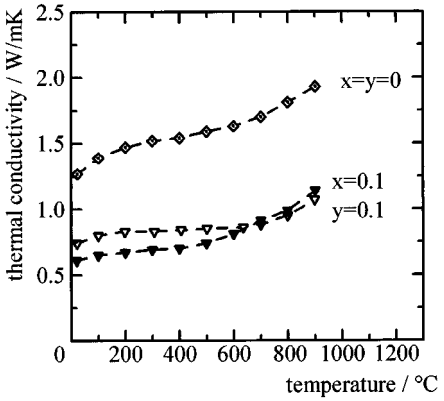

FIG. 12. Thermal conductivity for $(In_{1-x}Y_x)_4(Sn_{1-y}Ti_y)_3O_{12}$.

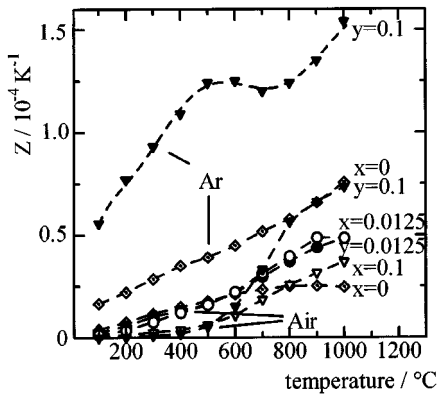

FIG. 13. Thermoelectric efficiency $Z = S^2\sigma/\kappa$ for $(In_{1-x}Y_x)_4(Sn_{1-y}Ti_y)_3O_{12}$ annealed in argon and air.

low values. Highly substituted compounds showed κ values of about half of that of the ternary compound despite their higher relative density of about 68%.

The thermoelectric figure of merit, Z, for the ternary compound annealed under air shows a maximum value of $2.5 \times 10^{-1}\,K^{-1}$ at 800°C, which is in agreement with the results of Ohtaki *et al.* (1) (see Fig. 13). In the high-temperature range we observed exceeding Z for weakly and for strongly substituted compounds with a high oxygen level. Annealing the compounds under argon atmosphere containing less than 10 ppm oxygen, Z is generally larger across the whole temperature range from room temperature up to 1273 K. A maximum Z of $1.5 \times 10^{-4}\,K^{-1}$ at 1273 K was observed for the $In_4(Sn_{0.9}Ti_{0.1})_3O_{12}$ compound.

CONCLUSIONS

The structure and the thermoelectric transport properties of *Me*-substituted $In_4Sn_3O_{12-\delta}$, $Me = Y$ and Ti, have been investigated. $In_4Sn_3O_{12}$ is isostructural with a wide range of M_7O_{12} compounds that exhibit a fluorite-related

superstructure. The *Me* ions were found to be located at the *M*2 (18*f*) position instead of In in the case of Y substitution and Sn in the case of Ti substitution. Y substitution causes an enlargement of the unit cell whereas Ti substitution diminishes the size of the unit cell.

In particular, the highly Ti-substituted compound annealed under argon at high temperatures exhibited large values of $S^2\sigma$. These results are attributed to both the high σ values and the increasing S values with increasing temperature up to 1273 K. The promising thermoelectric properties of $In_4(Sn_{0.9}Ti_{0.1})_3O_{12-\delta}$ are presumably due to ionic defect activation in the oxide together with large carrier mobility. κ of ternary $In_4Sn_3O_{12-\delta}$ was as low as $1.3\ W\ m^{-1}\ K^{-1}$ at room temperature reaching $1.9\ W\ m^{-1}\ K^{-1}$ at 1170 K. Highly *Me*-substituted compounds showed rather lower thermal conductivities, about half of that of the ternary compound despite their higher relative density influencing the σ and the κ value. The Ti-substituted compound consequently has $Z = 1.5 \times 10^{-4}\ K^{-1}$ as the maximum value at 1273 K. This is the largest Z value yet reported for metal oxides, which are considered as promising materials for high-temperature thermoelectric power generation because of their excellent durability in air.

ACKNOWLEDGMENTS

We thank Dr. N. Murayama of the National Industrial Research Institute of Nagoya for his kind cooperation in the laser flash measurement of thermal conductivity and I. Bächer of the Institute of Solid State and Materials Research Dresden for performing EBMA analysis. This work was partly supported by the Deutsche Forschungsgemeinschaft, contract number Pi282/2-1, funding the stay of W.P. at Nagoya University.

REFERENCES

1. L. D. Hicks and M. S. Dresselhaus, *Phys. Rev. B* **47,** 12727 (1993).
2. A. T. Burkov, A. Heinrich, C. Gladun, W. Pitschke, and J. Schumann, *Phys. Rev. B* **58,** 9644 (1998).
3. G. A. Slack, *in* "CRC Handbook of Thermoelectrics" (D. M. Rowe, Ed.), Chap. 34, p. 4074. Chemical Rubber, Boca Raton, FL, 1995.
4. B. C. Sales, D. Mandrus, B. C. Chakoumakos, V. Keppens, and J. R. Thompson, *Phys. Rev. B* **56,** 15081 (1997).
5. C. M. Bhandari and D. M. Rowe, *Contemp. Phys.* **21,** 219 (1980).
6 .J. C. Bass and N. B. Elsner, "Proc. 3rd Int. Conf. Therm. Energy," p. 8. Univ. of Texas at Arlington, Arlington, TX, 1980.
7. J. F. Nakahara, T. Takeshita, M. J. Tschetter, B. J. Beaudry, and K. A. Gschneidner, Jr., *J. Appl. Phys.* **63,** 2331 (1988).
8. I. Nishida and T. Sakata, *J. Phys. Chem. Sol.* **39,** 499 (1978).
9. H. Lange, *Phys. Stat. Sol. B* **201,** 3 (1997).
10. W. Pitschke, R. Kurt, A. Heinrich, J. Schumann, H. Griessmann, H. Vinzelberg, and A. T. Burkov, *J. Mater. Res.* **15,** 772 (2000).
11. C. Wood and D. Emin, *Phys. Rev. B* **29,** 4582 (1984).
12. S. Yugo, T. Sato, and T. Kumura, *Appl. Phys. Lett.* **46,** 842 (1985).
13. M. Yasukawa and N. Murayama, *J. Mater. Sci.* **31,** 6489 (1997).
14. W. J. Weber, C. W. Griffin, and J. L. Bates, *J. Am. Ceram. Soc.* **70,** 265 (1987).
15. M. Kazeoka, H. Hiramatsu, W.-S. Seo, and K. Koumoto, *J. Mater. Res.* **13,** 523 (1998).
16. M. Yasukawa and N. Murayama, *Mater. Sci. Eng. B* **54,** 64 (1998).
17. I. Terasaki, Y. Sasago, and K. Uchinokura, *Phys. Rev. B* **56,** 12685 (1997).
18. M. Ohtaki, D. Ogura, K. Eguchi, and H. Aral, *J. Mater. Chem.* **4,** 653 (1994).
19. J. L. Bates, C. W. Griffin, D. D. Marchant, and J. E. Garnier, *Am. Ceram. Soc. Bull.* **65,** 673 (1986).
20. G. Behr and G. Krabbes, "Abschlußbericht zum DFG-Förderprojekt Kr1241/1-1 und Be 1749/1-3," p. 67. Dresden, 1996.
21. H. Enoki, J. Echigoya, and H. Suto, *J. Mater. Sci.* **26,** 4110 (1991).
22. N. Nadaud, N. Lequex, M. Nanot, J. Jove, and T. Roisnel, *J. Solid State Chem.* **135,** 140 (1998).
23. M. R. Thornber and D. J. Bevan, *J. Solid State Chem.* **1,** 536 (1970).
24. R. A. Young, A. Sakthivel, T. S. Moss, C. O. Paiva-Santos, "Users guide to program DBWS-9411." Georgia Institute of Technology, Atlanta, GA, 1995.
25. R. A. Young and D. B. Wiles, *J. Appl. Crystallogr.* **12,** 430 (1982).
26. H. M. Rietveld, *J. Appl. Crystallogr.* **2,** 65 (1969).
27. F. H. Spedding, K. Gschneidner, Jr., and A. H. Daane, *J. Am. Chem. Soc.* **80,** 4499 (1958).
28. R. D. Shannon, *Acta Crystallogr., Sect. A: Cryst. Phys., Diffr., Theor. Gen. Crystallogr.* **32,** 751 (1976).
29. W. Fliegel, Doctoral thesis, Technological University Dresden, 1996.
30. N. Yamazoe, J. Fuchigami, M. Kishikawa, and T. Seiyama, *Surf. Sci.* **86,** 335 (1979).